Dielectric properties of liquid ethanol. A computer simulation study

Leonor Saiz
Departament de Física Fonamental, Universitat de Barcelona, Diagonal 647, E-08028 Barcelona, Spain

Elvira Guàrdia
Departament de Física i Enginyeria Nuclear, Universitat Politècnica de Catalunya, Sor Eulàlia D'Anzizu, Campus Nord, Mòdul B4-B5, E-08034 Barcelona, Spain

Joan-Àngel Padró
Departament de Física Fonamental, Universitat de Barcelona, Diagonal 647, E-08028 Barcelona, Spain

Static and dynamic dielectric properties of liquid ethanol have been studied as a function of the wave-vector number by computer simulation. Molecular dynamics simulations at room temperature have been performed using the optimized potentials for liquid simulations (OPLS) potential model proposed by Jorgensen [J. Phys. Chem. **90**, 1276 (1986)]. The time dependent correlation functions of the longitudinal and transverse components of the dipole density as well as the individual and total dipole moment autocorrelation functions have been calculated. The infrared spectra and the dielectric relaxation of the liquid have been also analyzed. Results have been compared with the available experimental data. Special attention has been dedicated to investigate the molecular origin of the different analyzed properties. © *2000 American Institute of Physics.* [S0021-9606(00)51531-1]

I. INTRODUCTION

The study of dielectric properties is fundamental for a deep understanding of polar liquids. Computer simulations provide a suitable tool to analyze these properties at molecular level, providing a direct route from microscopic details to macroscopic properties of experimental interest. The molecular dynamics (MD) simulation method is appropriate for this purpose since it enables one to obtain both static and dynamic properties. However, difficulties arise due to the slow relaxation of the time correlation functions of interest and to the sensitivity to the long-range intermolecular interactions of the quantities involved. To overcome the first difficulty, extremely long simulations should be performed whereas fairly large systems are required to overcome the latter. Moreover, statistically accurate calculations of these collective properties will also require very long simulations since only one value of a given collective quantity is obtained at each time step. In the case of polar protic systems, the study of dielectric properties is especially relevant due to the important role played by these fluids as solvents in chemistry (for a review on computer simulation of hydrogen bonded liquids, see Ref. 1). Among these liquids, water has focused the interest of most of the computer simulation studies. In the case of alcohols, only the dielectric properties of liquid methanol[2–4] and methanol–water mixtures[5] have been analyzed by computer simulation. Many experimental studies of both static and dynamic dielectric properties of hydrogen bonded liquids have been carried out, but in the case of ethanol, the latter are restricted to the microwave region of the spectra[6] and to the infrared region[7] up to about 34 cm^{-1}. To achieve a better understanding of the dielectric properties of monohydric alcohols, we show in this article the results

obtained for liquid ethanol by means of MD simulations. We have computed the static dielectric constant and the transverse and longitudinal components of the dielectric permittivity at different wave-vector numbers paying special attention to the low wave-vector limit, which provides an alternative route to calculate the dielectric permittivity. We have also determined the time correlation functions of the longitudinal and transverse components of the dipole density as a function of the wave-vector number, as well as the total dipole moment autocorrelation function and its self- and distinct components. In addition, the dielectric relaxation and the far infrared spectra have been investigated. It is worth emphasizing that previous computer simulations of liquid ethanol were restricted to the computation of individual properties at different thermodynamic states.[8–13]

The article is organized as follows. In Sec. II, a theoretical background is provided for the necessary definitions. Details of the simulations are given in Sec. III. Static dielectric properties are reported in Sec. IV. Section V is devoted to the results concerning dynamical dielectric properties, including time correlation functions and frequency spectra. The dynamics underlying the principal dielectric band in the microwave frequency region is analyzed. The infrared spectra is investigated in Sec. VI. Comparison between experimental and simulation data is presented throughout the article. The main results and conclusions are summarized in Sec. VII.

II. THEORETICAL FRAMEWORK

For an infinite system with cubic or spherical symmetry, the dielectric permittivity and susceptibility tensors are related through

J. Chem. Phys., Vol. 113, No. 7, 15 August 2000

Dielectric properties of liquid ethanol   2815

$$\frac{\epsilon_L(k,\omega)-\epsilon_\infty}{\epsilon_L(k,\omega)\epsilon_\infty}=\chi_L^0(k,\omega) \tag{1}$$

and

$$\epsilon_T(k,\omega)-\epsilon_\infty=\chi_T^0(k,\omega) \tag{2}$$

for the longitudinal and transverse components, respectively. ϵ_∞ is the dielectric constant at optical frequencies. (For a model system with nonpolarizable molecules, $\epsilon_\infty=1$.) Linear response theory relates the susceptibility tensor $\chi^0(\vec{k},\omega)$ to correlation functions of the Fourier components of the dipole density of the system $\vec{M}(\vec{k},t)$. The two components of $\vec{M}(\vec{k},t)$,

$$\vec{M}(\vec{k},t)=\vec{M}_L(\vec{k},t)+\vec{M}_T(\vec{k},t), \tag{3}$$

can be expressed as follows:

$$\vec{M}_L(\vec{k},t)=\sum_{j=1}^{N}\hat{k}\hat{k}\cdot\vec{\mu}_j(t)\exp(i\vec{k}\vec{r}_j^{\,\mathrm{CM}}(t)) \tag{4}$$

and

$$\vec{M}_T(\vec{k},t)=\sum_{j=1}^{N}(1-\hat{k}\hat{k})\cdot\vec{\mu}_j(t)\exp(i\vec{k}\vec{r}_j^{\,\mathrm{CM}}(t)), \tag{5}$$

where $\vec{\mu}_j(t)$ is the dipole moment of the jth molecule and $\vec{r}_j^{\,\mathrm{CM}}(t)$ the position of its center-of-mass. The components of the susceptibility tensor are given by[14,15]

$$\chi_A^0(k,\omega)=\frac{\langle|\vec{M}_A(\vec{k},0)|^2\rangle}{\nu_A V k_B T \epsilon_0}[1+i\omega\Phi_A(k,\omega)], \tag{6}$$

where $A=L$ or T (with $\nu_L=1$ and $\nu_T=2$), V is the volume of the sample, ϵ_0 is the vacuum permittivity, and $\Phi_A(k,\omega)$ is the Fourier transform,

$$\Phi_A(k,\omega)=\int_0^\infty dt\,\Phi_A(k,t)\exp(i\omega t), \tag{7}$$

of the normalized dipole density correlation function $\Phi_A(k,t)$ defined by

$$\Phi_A(k,t)=\frac{\langle\vec{M}_A(\vec{k},t)\cdot\vec{M}_A(-\vec{k},0)\rangle}{\langle|\vec{M}_A(\vec{k},0)|^2\rangle}. \tag{8}$$

Because of the short-ranged nature of the correlations which determine the dielectric permittivity, $\epsilon(k,\omega)$ must become independent of the wave-vector number when k is sufficiently small, that is

$$\lim_{k\to0}\epsilon_T(k,\omega)=\lim_{k\to0}\epsilon_L(k,\omega)=\epsilon(\omega). \tag{9}$$

The expressions for the components of the static wave-vector dependent dielectric constant can be deduced from Eqs. (1) and (2). For the static case, i.e., $\omega=0$, they reduce to

$$\frac{\epsilon_L(k)-\epsilon_\infty}{\epsilon_L(k)\epsilon_\infty}=y\frac{\langle|\vec{M}_L(\vec{k},0)|^2\rangle}{N\mu^2} \tag{10}$$

and

$$\epsilon_T(k)-\epsilon_\infty=y\frac{\langle|\vec{M}_T(\vec{k},0)|^2\rangle}{2N\mu^2}, \tag{11}$$

where

$$y=\frac{\rho\mu^2}{k_B T\epsilon_0}, \tag{12}$$

with ρ the molecular number density and μ the molecular dipole moment. Another quantity of interest,[16] $\epsilon^R(k)$, results by dividing both sides of Eqs. (10) and (11)

$$\epsilon^R(k)=\frac{\langle|\vec{M}_T(\vec{k},0)|^2\rangle}{2\langle|\vec{M}_L(\vec{k},0)|^2\rangle}, \tag{13}$$

or equivalently

$$\epsilon^R(k)=\frac{x_T(k)}{x_L(k)}, \tag{14}$$

where

$$x_T(k)=\frac{\langle|\vec{M}_T(\vec{k},0)|^2\rangle}{2N\mu^2} \tag{15}$$

and

$$x_L(k)=\frac{\langle|\vec{M}_L(\vec{k},0)|^2\rangle}{N\mu^2}. \tag{16}$$

In the low k limit the following condition must be fulfilled:

$$\lim_{k\to0}\epsilon_L(k)=\lim_{k\to0}\epsilon_T(k)=\epsilon. \tag{17}$$

Alternatively,

$$\lim_{k\to0}\epsilon^R(k)=\epsilon. \tag{18}$$

Equations (9) and (17) provide a route to determine $\epsilon(\omega)$ and ϵ, respectively. However, due to the periodic boundary conditions used during the computer simulations, the k vectors which may be studied are restricted to

$$\vec{k}=\frac{2\pi}{L}(l,m,n), \tag{19}$$

where l, m, n are integers and L is the length of the cubic box. Thus, the smallest wave-vector which may be studied is $k_{\min}=2\pi/L$. Whether the low k limit is reached can be tested through the consistency of the calculated $\epsilon_L(k_{\min},\omega)$ and $\epsilon_T(k_{\min},\omega)$. Another approach for the determination of $\epsilon(\omega)$ is based on the calculation of the total dipole moment of the primitive cube of the simulation $\vec{M}(t)=\Sigma_{j=1}^N\vec{\mu}_j(t)$. If the Ewald summation technique is used to handle with the long-range interactions and conducting walls boundary conditions are assumed, the relation between $\epsilon(\omega)$ and the total dipole moment correlation is given by[17,18]

$$\epsilon(\omega)-\epsilon_\infty=\frac{\langle|\vec{M}(0)|^2\rangle}{3Vk_BT\epsilon_0}[1+i\omega\Phi(\omega)], \tag{20}$$

where $\Phi(\omega)$ is the Fourier transform of the $\vec{M}$ autocorrelation function

$$\Phi(t) = \frac{\langle \vec{M}(t) \cdot \vec{M}(0) \rangle}{\langle |\vec{M}(0)|^2 \rangle}. \qquad (21)$$

Finally, the static dielectric constant is given by

$$\epsilon = \epsilon_\infty + \frac{y}{3} G_k, \qquad (22)$$

where G_k is the finite system Kirkwood correlation factor

$$G_k = \frac{\langle |\vec{M}(0)|^2 \rangle}{N\mu^2}. \qquad (23)$$

G_k accounts for the correlations of the total dipole moment. It can be expressed as

$$G_k = \frac{\langle |\vec{M}(0)|^2 \rangle}{N\mu^2} = 1 + \frac{N-1}{\mu^2} \langle \vec{\mu}_i \cdot \vec{\mu}_j \rangle, \qquad (24)$$

where the averages of the product $\vec{\mu}_i \cdot \vec{\mu}_j$ are performed for different molecules ($i \neq j$). G_k reflects the degree of correlation between the orientation of neighboring molecules. So, $G_k = 1$ if there is no correlation, $G_k > 1$ when molecular dipole moments tend to orient themselves parallel to each other, and $G_k < 1$ when molecular dipole moments tend to orient themselves in opposite directions. Once ϵ has been obtained from Eq. (22) the Kirkwood factor g_k which describes orientational correlations in an infinite sample may be obtained by means of the relationship

$$g_k = \frac{(2\epsilon + \epsilon_\infty)}{3\epsilon} G_k. \qquad (25)$$

III. COMPUTER SIMULATION DETAILS

Molecular dynamics simulations of liquid ethanol were performed at room temperature ($T = 298$ K) and the experimental density at normal pressure ($d = 0.7873$ g/cm^3). The number of molecules in the central box was $N = 125$, which corresponds to a cubic box of side length $L = 22.99$ Å. Periodic boundary conditions were used. We adopted the optimized potentials for liquid simulations (OPLS) potential and the molecular model proposed by Jorgensen in Ref. 8. Each ethanol molecule consists of four interaction sites corresponding to the two methyl groups and the oxygen and the hydrogen atoms of the hydroxyl group. Hydrogen atoms of the methyl groups are not explicitly considered. Bond lengths and bond angles are kept constant, and the only intramolecular motions considered in the simulations are the torsions around the central C–O bond. Interactions between sites are described by Lennard-Jones and Coulomb terms. The partial charges and molecular geometry yield a molecular dipole moment $\mu = 2.22$ D (1 D $= 3.335 \times 10^{-30}$ ccm) that is significantly larger than the experimental gas-phase value[19] $\mu_{gas} = 1.69$ D. In recent work,[11,13] it has been shown that the OPLS potential reproduces fairly well the thermodynamic properties, the structure, and single particle dynamics of liquid ethanol at different thermodynamic states.

The equations of motion were integrated using the algorithm proposed by Berendsen and co-workers in Ref. 20, which consists of a leap-frog Verlet algorithm with a weak

TABLE I. Static dielectric constant and Kirkwood g factor.

Method	G_k	ϵ	ϵ_∞	$\epsilon - \epsilon_\infty$	g_k
This work[a]	2.9 ± 0.4	16 ± 2	1	15 ± 2	2.0 ± 0.2
Expt.[b]		24.32	2.69	21.63	
Expt.[c]		24.35	1.93	22.42	

[a]Statistal errors have been computed following the blocking method of Ref. 23.
[b]Reference 6.
[c]Reference 7.

coupling to a thermal bath. We used a time step of 2.5 fs. Constraints were handled by means of the SHAKE method.[21] We performed two MD runs consisting of an initial equilibration period of about 100 ps and an equilibrium period of 1300 ps during which the properties were calculated. The results reported in the next sections are the average of those obtained from these two independent runs. The short-range forces were truncated at half the box length and the Ewald summation with conducting boundary conditions[22] was used for Coulomb interactions.

IV. STATIC DIELECTRIC PROPERTIES

Let us first examine the static properties obtained from the MD simulations following the scheme described previously. To this purpose we consider the more relevant quantities, namely, the Kirkwood correlation factor, the static dielectric constant, and the longitudinal and transverse wave-vector dependent static dielectric constants.

A. $k=0$ properties

As discussed in Sec. II, one of the approaches to the computation of the static dielectric constant by MD simulations is from Eqs. (22), (23), and (25) (in our case $y = 15.49$). The values of G_k, ϵ, and g_k found in this way are given in Table I and they are compared with the available experimental data. The Kirkwood g factor G_k obtained from MD was greater than 1, as expected since there is a parallel alignment of the dipole moments of near-neighboring molecules.[11] The convergence of the cumulative average of the static dielectric constant as a function of the simulation
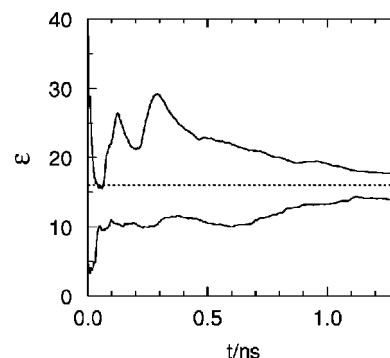

FIG. 1. Convergence of the static dielectric constant as a function of the simulation length for each run. The dashed line corresponds to the final value of ϵ obtained by averaging the two runs.

TABLE II. Longitudinal and transverse components of the wave-vector dependent static dielectric constant.

$(k/k_{min})^2$	$k/\text{Å}^{-1}$	$x_L(k)$	$x_T(k)$	$\epsilon_L(k)$	$\epsilon_T(k)$	$\epsilon^R(k)$
1	0.273	0.0581 ± 0.0008	0.93 ± 0.45	10.0 ± 1.2	15.5 ± 0.7	16.1 ± 0.5
2	0.386	0.0605 ± 0.0003	0.80 ± 0.01	15.9 ± 1.2	13.3 ± 0.1	13.2 ± 0.1
3	0.473	0.0656 ± 0.0004	0.65 ± 0.02	-62.3 ± 24.1	10.1 ± 0.3	9.98 ± 0.2
6	0.669	0.0960 ± 0.0006	0.490 ± 0.005	-2.05 ± 0.04	8.58 ± 0.08	5.10 ± 0.02
9	0.819	0.136 ± 0.001	0.394 ± 0.003	-0.90 ± 0.01	7.10 ± 0.05	2.902 ± 0.001

length is plotted in Fig. 1. This picture shows that the MD simulations are long enough to reach a plateau value for ϵ and that this plateau value is quite sensitive to the initial conditions. The value obtained by averaging the two runs, i.e., $\epsilon=16\pm2$, is lower than the experimental data, but the agreement is similar to that achieved for liquid methanol.[2–4] Since part of the discrepancies are due to the value of the high-frequency dielectric constant, we find it more significant to compare the difference $(\epsilon-\epsilon_\infty)$. In this case, the agreement between experimental and MD simulation results is better. It should be noticed that the experimental value of ϵ_∞ corresponds to a polarizable system (i.e., the real fluid), whereas the simulations have been carried out with a system of nonpolarizable molecules for which $\epsilon_\infty=1$.

B. Wave-vector dependent dielectric constant

The other approach to the computation of the static dielectric constant is from the low k limit of the longitudinal and transverse components of the permittivity tensor. In this study, $k_{min}=0.273$ Å^{-1}. We have calculated the wave-vector dependent quantities for the three smallest k values, namely, $k=k_{min}$, $\sqrt{2}k_{min}$, and $\sqrt{3}k_{min}$, as well as for $k=\sqrt{6}k_{min}$ and $3k_{min}$. The values of x_L and x_T found from the MD simulations by using Eqs. (15) and (16), the resulting $\epsilon_L(k)$ and $\epsilon_T(k)$ components of the permittivity tensor computed from Eqs. (10) and (11) and the $\epsilon^R(k)$ values computed from Eq. (14) are collected in Table II. The statistical errors have been evaluated by using the blocking method as described in Ref. 23. The general trends found in the k dependence of the $\epsilon_T(k)$ and $\epsilon_L(k)$ functions agree with previous theoretical results for model polar liquids.[24–26] In the low k limit, we can see that the relation $\epsilon_T(k_{min})\simeq\epsilon\simeq\epsilon^R(k_{min})$ is satisfied within the statistical errors. The good agreement between the results obtained following the two approaches to the calculation of ϵ is an indication that the size of the simulated system is sufficiently large to be considered as representing a real isotropic fluid. As was already pointed out by Fonseca and Ladanyi,[2] $\epsilon_T(k)$ provides a route much better than $\epsilon_L(k)$ to determine the dielectric permittivity. While $\epsilon_T(k)$ is a slowly varying function of k near $k=0$, the transition $\epsilon_L(k\to0)\simeq\epsilon$ occurs very sharply. Furthermore, $\epsilon_L(k)$ has a singularity at $x_L(k)=1/y$ and it is negative for $yx_L(k)<1$ [see Eq. (10)]. As we can see in Table II, we have been able to obtain $\epsilon_L(k)$ for values of k lower and higher than that corresponding to this singularity. To the best of our knowledge the only previous computer simulation results showing the divergence of $\epsilon_L(k)$ at small k are those reported for liquid water in a recent work of Bopp et al.[27]

V. DYNAMIC DIELECTRIC PROPERTIES

In this section we are concerned with the calculation of the dipole density time correlation functions and their power spectra. Special attention has been dedicated to the investigation of the origin of the different contributions to the total dipole moment autocorrelation function. A thorough comparison with experimental dielectric relaxation data, where collective motions are of special interest, has been also performed.

A. Dipole density time correlation functions

The normalized time correlation functions of the longitudinal $\Phi_L(k,t)$ and transverse $\Phi_T(k,t)$ components of the dipole density defined by Eq. (8) have been computed during the MD simulations for the five k values listed above. In Figs. 2 and 3, the $\Phi_L(k,t)$ and $\Phi_T(k,t)$ functions are plotted and a detail of the short-time regime is provided in the inset. The $\Phi(t)$ function resulting from the MD simulations, as well as its different contributions are represented in Fig. 4.

The relaxation of the longitudinal dipole density plays a central role in solvation dynamics.[28] As can be seen from Fig. 2, the main feature of $\Phi_L(k,t)$ is a fast initial decay with a strongly oscillatory character. The same behavior was previously observed for methanol[4] and water.[29] The initial decay of $\Phi_L(k,t)$ has been attributed to inertial and librational dynamics.[30] It is worthy to note that other polar nonhydrogen bonded liquids show a fast decay of $\Phi_L(k,t)$ to zero and then overdamped oscillations.[16]
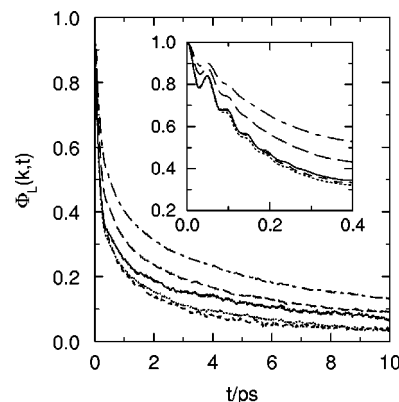

FIG. 2. Normalized time correlation function of the longitudinal component of the dipole moment density for $(k/k_{min})^2=1$ (full line), $(k/k_{min})^2=2$ (dotted line), $(k/k_{min})^2=3$ (dashed line), $(k/k_{min})^2=6$ (long dashed line), and $(k/k_{min})^2=9$ (dotted–dashed line). The inset shows the short-time behavior of $\Phi_L(k,t)$.
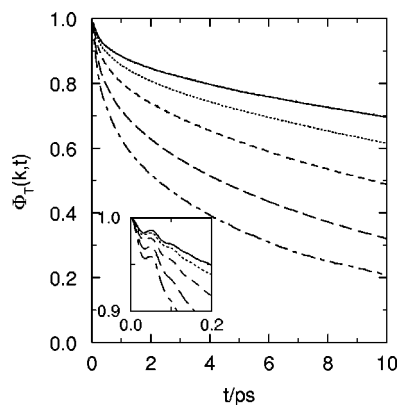
FIG. 3. Same as Fig. 2 for the transverse component of the dipole moment density $\Phi_T(k,t)$.

Comparison of Figs. 2 and 3 reveals important differences in the relaxation of the transverse and longitudinal components of the dipole density. The decay of the transverse component is slower than that of its longitudinal counterpart. On the other hand, the behavior of the $\Phi_T(k,t)$ functions is similar to that of the total dipole moment autocorrelation function $\Phi(t)$ (see Figs. 3 and 4).

For the transverse and total functions displayed in Figs. 3 and 4, it is possible to distinguish three separate regimes. The long-time regime which takes place for $t>1.5$ ps can be modeled as an exponential function and describes the relaxation of the principal dielectric band of $\Phi_T(k,t)$ and $\Phi(t)$. This regime takes place when inertial and librational dynamics do not contribute appreciably to the collective reorientation. The short-time regime, i.e., for $t<0.5$ ps, which is shown in detail in the inserts of Figs. 3 and 4, has a fast initial inertial decay and then an oscillatory behavior which is related to the librational dynamics of the molecule. The oscillatory behavior is characteristic of hydrogen bonded liquids and it is absent in polar liquids without hydrogen bonding interactions such as acetonitrile.[16] The fast initial decay and the oscillatory behavior are both mainly due to the individual particle reorientation. This aspect will be discussed in more detail in Sec. V B. The intermediate regime can also be modeled as an exponential function but with a characteristic time smaller than the one corresponding to the long-time regime. The large and intermediate regimes for the different ψ functions, where ψ is any of the $\Phi(t)$ or $\Phi_T(k,t)$ correlation functions, have been fitted to a function of the type

$$\psi(t) \sim \sum_{j=1}^{2} A_j \exp(-t/\tau_j), \quad t>0.5 \text{ ps.} \tag{26}$$

For the whole time interval considered, these functions can be expressed by

$$\psi(t) \sim \sum_{j=1}^{2} A_j \exp(-t/\tau_j) + \left(1 - \sum_{j=1}^{2} A_j\right) \phi_{\text{librational-inertial}}(t). \tag{27}$$

The fitted parameters are summarized in Table III. We observe that the amplitude A_1 of the main relaxation process decreases with increasing k, while that of the second process A_2 increases. Both relaxation times decrease as k increases, but the dependence on k is much more important in the case of τ_1 than for τ_2. On the other hand, the relaxation times corresponding to $\Phi_T(k_{\min},t)$ are smaller than those of $\Phi(t)$. The difference is specially significant in the case of τ_1.

The so-called Debye relaxation time τ_D is also reported in Table III. It was obtained from the following expression:[31]

$$\tau_D = \lim_{\omega \to 0} \frac{\epsilon - \epsilon(\omega)}{i\omega[\epsilon(\omega) - \epsilon_\infty]}. \tag{28}$$

For a Debye dielectric[32] it should be $\tau_D \simeq \tau_1$. According to the results given in Table III, liquid ethanol does not behave like a Debye fluid since τ_D is significantly lower than τ_1.

B. Self- and distinct contributions to the total dipole moment autocorrelation function

Decomposing $\langle \vec{M}(t) \cdot \vec{M}(0) \rangle$ into its components arising from the correlations of the dipole moment of a molecule and the correlations between distinct (different) molecular dipole moments, one obtains the following expression for $\Phi(t)$ [see Eq. (21)]

$$\Phi(t) = \frac{N\mu^2}{\langle |\vec{M}(0)|^2 \rangle} \Phi_s(t)$$
$$+ \frac{N(N-1)\mu^2 \langle \vec{\mu}_i(0) \cdot \vec{u}_j(0) \rangle}{\langle |\vec{M}(0)|^2 \rangle} \Phi_d(t), \tag{29}$$

where $\Phi_s(t)$ is the reorientational autocorrelation function of the individual dipoles and can be expressed by

$$\Phi_s(t) = \frac{\langle \vec{\mu}_i(t) \cdot \vec{\mu}_i(0) \rangle}{\langle |\vec{\mu}_i(0)|^2 \rangle} = \langle \vec{u}_i(t) \cdot \vec{u}_i(0) \rangle, \tag{30}$$

TABLE III. Two-exponential fit parameters for the dipole density time correlation functions resulting from MD simulations [components: self, total, and transverse (T)], Debye relaxation time, and single-particle correlation time.

Component	$(k/k_{\min})^2$	A_1	τ_1/ps	A_2	τ_2/ps	τ_D/ps	τ_s/ps
Self	0	0.731	26.0	0.105	1.50		20
Total	0	0.871	60.5	0.075	1.60	49	
T	1	0.861	46.5	0.080	1.50		
T	2	0.834	32.8	0.105	1.30		
T	3	0.785	20.9	0.125	1.25		
T	6	0.693	12.9	0.181	1.20		
T	9	0.575	9.70	0.250	1.18		

J. Chem. Phys., Vol. 113, No. 7, 15 August 2000

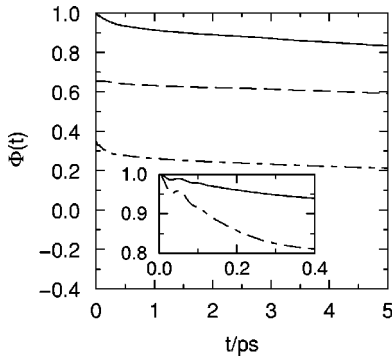Dielectric properties of liquid ethanol   2819

FIG. 4. Normalized total dipole moment autocorrelation function $\Phi(t)$ (solid line), self-contribution $G_k^{-1}\Phi_s(t)$ (dotted–dashed line), and distinct contribution $(1-G_k^{-1})\Phi_d(t)$ (long dashed line). The inset shows the short-time behavior of $\Phi(t)$ (full line) and $\Phi_s(t)$ (dotted–dashed line).

with $\vec{u}_i(t)$ a unit vector along the molecular dipole moment, $\vec{\mu}_i(t)=\mu\vec{u}_i(t)$. The $\Phi_d(t)$ function is given by

$$\Phi_d(t)=\frac{\langle\vec{u}_i(t)\cdot\vec{u}_j(0)\rangle}{\langle\vec{u}_i(0)\cdot\vec{u}_j(0)\rangle}, \quad i\neq j, \tag{31}$$

and, using Eq. (23),

$$\langle\vec{u}_i(0)\cdot\vec{u}_j(0)\rangle=\frac{G_k-1}{N-1}, \quad i\neq j. \tag{32}$$

Thus, Eq. (29) can be written as

$$\Phi(t)=\frac{1}{G_k}\Phi_s(t)+\left(1-\frac{1}{G_k}\right)\Phi_d(t). \tag{33}$$

In our system, the prefactors of the self and distinct contributions are $(1/G_k)=0.34\pm0.02$ and $(1-1/G_k)=0.65\pm0.02$, respectively. Thus, the main contribution to $\Phi(t)$ corresponds to the correlations among different molecular dipoles.

Figure 4 shows the two contributions to $\Phi(t)$. In the inset of the same figure we show the short-time behavior of the total and self-autocorrelation functions. The self-component for short times consists of a fast initial inertial decay with oscillations due to librational dynamics. For longer times, $\Phi_s(t)$ shows a nearly exponential decay. The long-time decay of $\Phi_s(t)$ is faster than that of the total dipole moment autocorrelation function $\Phi(t)$. The distinct component for short times does not present a fast inertial decaying behavior. Yet, $\Phi_d(t)$ decays more slowly than $\Phi_s(t)$. Therefore, the behavior of $\Phi(t)$ at long times will be dominated by $\Phi_d(t)$. Thus, the long-time behavior of $\Phi(t)$ should be associated with collective motions.

As expected, the relaxation times τ_1 and τ_2 found for $\Phi_s(t)$ according to Eq. (26) are smaller than those corresponding to $\Phi(t)$ (see Table III). Also given in Table III is the single-particle correlation time τ_s defined as

$$\tau_s=\int_0^\infty\Phi_s(t)\,dt. \tag{34}$$

The relation between the total and single-particle correlation times is interesting from a theoretical point of view. Accord-

TABLE IV. Dielectric relaxation parameters obtained from fitting three superimposed Debye equations to the experimental $\epsilon'(\omega)$ and $\epsilon''(\omega)$ data of liquid ethanol at room temperature.

	g_1	g_2	g_3	τ_1/ps	τ_2/ps	τ_3/ps
Ref. 6	0.917	0.031	0.052	163	8.97	1.81
Ref. 7	0.901	0.064	0.035	161	3.3	0.22

ing to our findings, liquid ethanol approximately obeys the Kivelson–Madden relationship[14] $\tau_D/\tau_s\simeq G_k$.

C. Dielectric relaxation

Dielectric relaxation of hydrogen bonded liquids has been extensively studied by experimental techniques. Data for liquid ethanol at room temperature are available in the microwave zone (up to 3 cm^{-1}) of the spectra[6] and up to frequencies of THz (34 cm^{-1}) reaching the far infrared region.[7] The experimental dielectric relaxation provides information on the real and imaginary parts of the frequency dependent permittivity $\epsilon(\omega)=\epsilon'(\omega)-i\epsilon''(\omega)$. In the case of monohydric alcohols, experimental data are usually analyzed by considering an empirical model which consists of three Debye-type processes.[33] With this assumption, $\epsilon(\omega)$ can be separated into the real and imaginary parts

$$\epsilon'(\omega)=\epsilon_\infty+(\epsilon-\epsilon_\infty)\sum_{j=1}^n\frac{g_j}{[1+(\omega\tau_j)^2]} \tag{35}$$

and

$$\epsilon''(\omega)=(\epsilon-\epsilon_\infty)\sum_{j=1}^n\frac{g_j(\omega\tau_j)}{[1+(\omega\tau_j)^2]}, \tag{36}$$

respectively. In Eqs. (35) and (36), τ_j are the relaxation times and $g_j=(\epsilon_j-\epsilon_{\infty j})/(\epsilon-\epsilon_\infty)$, $\epsilon_{\infty j}=\epsilon_{j+1}$, are the weights of processes j contributing to the total dispersion, beginning at the static permittivity $\epsilon=\epsilon_1$ and ending at the extrapolated high frequency permittivity ϵ_∞ $=\lim_{\omega\to\infty}\epsilon'(\omega)$.

The two available sets of experimental dielectric relaxation parameters for liquid ethanol at room temperature are listed in Table IV. It is worthy to note that Kindt and Schmuttenmaer[7] obtained significantly faster relaxation times for the second and third Debye processes than those reported by Barthel and co-workers.[6] The τ_j relaxation times are comparable to the values reported in Table III for the total dipole moment autocorrelation function. In general, the relaxation times resulting from MD are smaller than the experimental estimations. The disagreement is especially significant in the case of the main dispersion τ_1 value. A similar discrepancy was observed in the case of methanol.[3,4] On the other hand, the τ_2 value resulting from $\Phi(t)$ is quite close to the second relaxation time given in Ref. 7. According to our findings, the relaxation time corresponding to the third Debye process cannot be determined from the decay of $\Phi(t)$. This is probably due to the very different order-of-magnitude of τ_3 and τ_1. It should thus be determined from the decay of a function directly related to the physical origen of the corresponding relaxation process (see, for instance, Ref. 34).
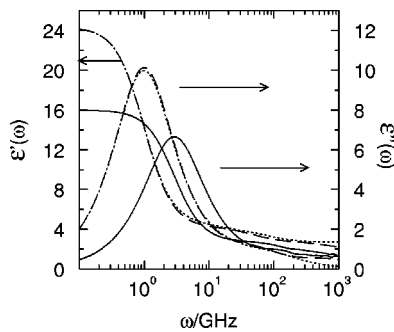
FIG. 5. Real $\epsilon'(\omega)$ and imaginary $\epsilon''(\omega)$ parts of the frequency dependent permittivity. Molecular dynamics results (solid line), experimental data from Ref. 6 (dotted line) and from Ref. 7 (dashed line). Experimental lines are calculated from the parameters of Table IV. The arrows indicate the vertical scale corresponding to each curve.

The MD results for $\epsilon'(\omega)$, $\epsilon''(\omega)$ and the corresponding Cole–Cole plot are compared with the experimental data in Figs. 5 and 6, respectively. The deviation of the Cole–Cole plot from a semicircle confirms that liquid ethanol is not a Debye fluid. In the high frequency region of the Cole–Cole plot, MD results exhibit the typical loops characteristic of fast librational motions. The dependence of the permittivity with frequency is qualitatively reproduced by the MD results, but we can observe some quantitative disagreements between the simulation results and experimental data. These disagreements are partly due to the discrepancies in the values of the static permittivity and the permittivity at optical frequencies. In Figs. 7 and 8, this is overcome by plotting the quantities $(\epsilon'(\omega)-\epsilon_\infty)/(\epsilon-\epsilon_\infty)$ and $\epsilon''(\omega)/(\epsilon-\epsilon_\infty)$. The discrepancies are now effectively reduced. The disagreements in the decay of the $(\epsilon'(\omega)-\epsilon_\infty)/(\epsilon-\epsilon_\infty)$ function as well as in the position of the peak of $\epsilon''(\omega)/(\epsilon-\epsilon_\infty)$ are directly related to the small value of the first relaxation time τ_1 resulting from MD. The discrepancies in the value of the second relaxation time τ_2 originate the differences observed in the intermediate frequency region of the Cole–Cole plot.

VI. INFRARED ABSORPTION

The experimental infrared absorption spectrum of a system is given in terms of the infrared absorption coefficient
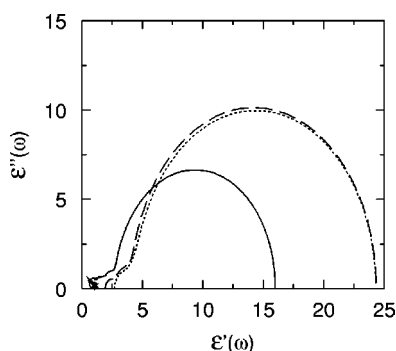

FIG. 6. Cole–Cole plot of the frequency dependent permittivity. Molecular dynamics results (solid line), experimental data from Ref. 6 (dotted line) and from Ref. 7 (dashed line). Experimental lines are calculated from the parameters of Table IV.
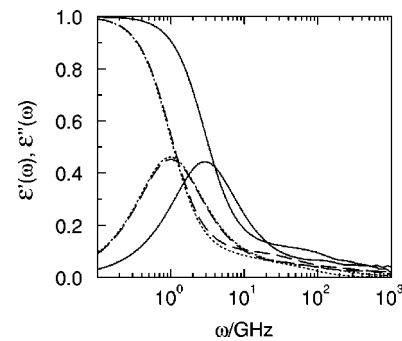

FIG. 7. Same as Fig. 5 with the real and imaginary parts of $\epsilon(\omega)$ scaled as $(\epsilon'(\omega)-\epsilon_\infty)/(\epsilon-\epsilon_\infty)$ and $\epsilon''(\omega)/(\epsilon-\epsilon_\infty)$, respectively.

$\alpha(\omega)$ and the imaginary part $\epsilon''(\omega)$ of the frequency dependent dielectric constant. These quantities are related to the absorption line shape, $I(\omega)$, by[35]

$$\alpha(\omega)=\frac{4\pi^2\omega}{3Vhcn(\omega)}[1-\exp(-\beta\hbar\omega)]I(\omega),\qquad(37)$$

$$\epsilon''(\omega)=\frac{c\alpha(\omega)n(\omega)}{\omega}=\frac{4\pi^2}{3Vh}[1-\exp(-\beta\hbar\omega)]I(\omega),\qquad(38)$$

where $\beta=(k_BT)^{-1}$, $\hbar=h/2\pi$, h is the Planck constant, c is the speed of light in vacuum, $n(\omega)$ is the refractive index of the medium, and $I(\omega)$ is the Fourier transform of the unnormalized total dipole moment autocorrelation function

$$I(\omega)=\frac{1}{2\pi}\int_{-\infty}^{\infty}dt\langle\vec{M}(t)\cdot\vec{M}(0)\rangle\exp(-i\omega t).\qquad(39)$$

For classical systems, $\langle\vec{M}(t)\cdot\vec{M}(0)\rangle$ is real and symmetric, and $I(\omega)$ can be written as

$$I(\omega)=\frac{1}{\pi}\int_0^{\infty}dt\langle\vec{M}(t)\cdot\vec{M}(0)\rangle\cos(\omega t).\qquad(40)$$

Equations (37), (38), and (40) can be used to relate infrared data with MD results. In the classical limit ($\hbar\to0$), Eq. (38) has the following form:

$$\epsilon''(\omega)=\frac{c\alpha(\omega)n(\omega)}{\omega}=(\epsilon-\epsilon_\infty)\omega\int_0^{\infty}dt\,\Phi(t)\cos(\omega t),\qquad(41)$$
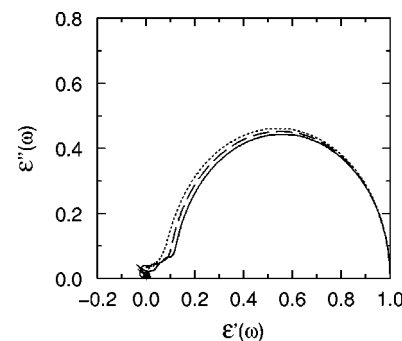

FIG. 8. Same as Fig. 6 with the real and imaginary parts of $\epsilon(\omega)$ scaled as $(\epsilon'(\omega)-\epsilon_\infty)/(\epsilon-\epsilon_\infty)$ and $\epsilon''(\omega)/(\epsilon-\epsilon_\infty)$, respectively.
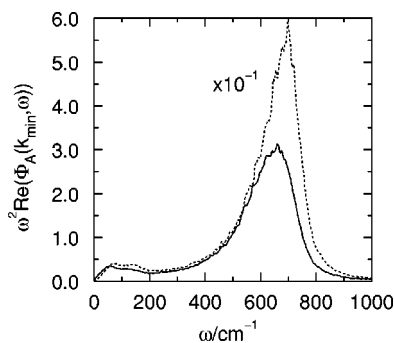
FIG. 9. ω^2 times the real part of the transverse (solid line) and longitudinal (dotted line) components of the dipole moment density spectrum for $k = k_{min}$. Notice that the curve corresponding to $\Phi_L(k_{min},\omega)$ has been multiplied by 0.1.

where $\Phi(t)$ is defined by Eq. (21) and we have used the definition of ϵ given in Eq. (22). Since we are concerned with frequencies higher than that of the principal dispersion band, we neglect the frequency dependence of the refractive index[36] to write

$$\alpha(\omega) \propto \omega \epsilon''(\omega) \propto \omega^2 \, \text{Re} \, (\Phi(\omega)). \qquad (42)$$

An alternative procedure to calculate $\alpha(\omega)$ is through the $k \to 0$ limits of $\epsilon_L(k,\omega)$ and $\epsilon_T(k,\omega)$. As in the $\omega=0$ case (see Sec. IV B), the most straightforward route to $\epsilon''(\omega)$ is provided by the transversal component. In the $k \to k_{min}$ limit, Eqs. (2) and (6) lead to

$$\epsilon''(\omega) \simeq \text{Im} \, (\epsilon_T \, (k_{min},\omega)) \propto \omega \, \text{Re} \, (\Phi_T(k_{min},\omega)). \qquad (43)$$

The absorption coefficient is thus proportional to $\omega^2 \, \text{Re} \, (\Phi_T(k_{min},\omega))$. Due to the ω^2 factor, $\alpha(\omega)$ emphasizes the high frequency part of the spectra. Resonant motions lead to maxima in the absorption coefficient whereas exponential relaxations result in slowly increasing functions that reach a constant value for frequencies larger than the inverse of the characteristic time.

The MD results for $\omega^2 \, \text{Re} \, (\Phi_T(k_{min},\omega))$ and $\omega^2 \, \text{Re} \, (\Phi(\omega))$ are depicted in Figs. 9 and 10, respectively. In Fig. 9, the $\omega^2 \, \text{Re} \, (\Phi_L(k_{min},\omega))$ function is also plotted for the sake of completeness. The $\omega^2 \, \text{Re} \, (\Phi_T(k_{min},\omega))$ spectrum exhibits a broad maximum at frequencies located between 500
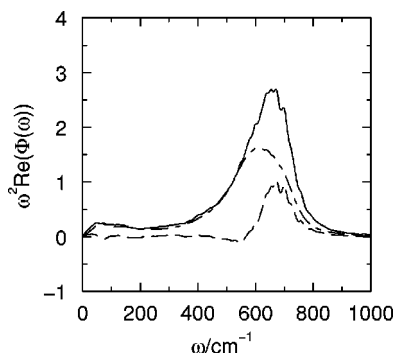

FIG. 10. ω^2 times the real part of the power spectrum of the total dipole moment autocorrelation function (solid line), self-contribution $G_k^{-1}\omega^2\Phi_s(\omega)$ (dotted–dashed line), and distinct contribution $(1-G_k^{-1})\omega^2\Phi_d(\omega)$ (dashed line).

and 750 cm^{-1} with a peak at approximately 640 cm^{-1}. Similar characteristics are shown by the $\omega^2 \, \text{Re} \, (\Phi_L(k_{min},\omega))$ function in the same region. However, the maximum is located at slightly higher frequencies ($\sim$690 cm^{-1}). On the other hand, the very good agreement between $\omega^2 \, \text{Re} \, (\Phi_T(k_{min},\omega))$ and $\omega^2 \, \text{Re} \, (\Phi(\omega))$ corroborates that the $k \to 0$ limit has effectively been reached in our simulations. To the best of our knowledge, there are not experimental infrared data to compare with our results. Experimental data corresponding to liquid methanol display a maximum at similar frequencies (around 570 cm^{-1} according to Ref. 37 and around 700 cm^{-1} according to Ref. 38).

To gain insight into the dynamic origin of the spectral features, we have analyzed the self- and distinct contributions to $\alpha(\omega)$. By using Eq. (33), we obtain the following relation

$$\omega^2\Phi(\omega) = \frac{1}{G_k}\omega^2\Phi_s(\omega) + \left(1 - \frac{1}{G_k}\right)\omega^2\Phi_d(\omega). \qquad (44)$$

As can be seen from Fig. 10, the self-contribution $G_k^{-1}\omega^2 \, \text{Re} \, (\Phi_s(\omega))$ has a broad band in the infrared region located between 400 and 800 cm^{-1}, with a maximum at $\sim$600 cm^{-1}. This frequency corresponds to an oscillation with a characteristic time of 0.05 ps. This high frequency maximum can be assigned to librational motions of the hydroxyl H atoms around the central methyl–oxygen bond and, more specifically, to hydrogen bonded molecules. This assumption is supported by a previous analysis of the spectral densities in the liquid.[11] This analysis shows that the power spectrum of the velocity autocorrelation function of H-bonded hydrogen atoms has a band whose maximum is around 630 cm^{-1}, while the H atoms that do not participate in a hydrogen bond give a band whose maximum is around 370 cm^{-1}. Because of the very low percentage of nonbonded molecules,[11] this band at intermediate frequencies can not be appreciated in Fig. 10.

The $G_k^{-1}\omega^2 \, \text{Re} \, (\Phi_s(\omega))$ function also presents a maximum at low frequencies in the far infrared zone of the spectra. This peak is located at about 70 cm^{-1}. It corresponds to an oscillation with a characteristic time ten times greater than the previous one ($\sim$0.5 ps). In the case of water, the peak found in this frequency range has been ascribed to different physical origins, namely, hindered motions of the molecules in the cage formed by its neighbors,[39] induced dipole contributions,[40] and bending vibrations of the hydrogen bonds (O···O···O units).[41] In our ethanol simulations, dipole induced contributions have not been taken into account. On the other hand, a maximum at about 70 cm^{-1} also appears in the power spectra of the velocity autocorrelation functions of the oxygen atoms of liquid ethanol, and this maximum is independent of the hydrogen bonding state of the molecule.[11] We may then conclude that the low frequency peak shown by $G_k^{-1}\omega^2 \, \text{Re} \, (\Phi_s(\omega))$ can be ascribed to hindered motions of the molecules in the cage formed by its neighbors.

The distinct component $(1-G_k^{-1})\omega^2 \, \text{Re} \, \Phi_d(\omega)$ (see Fig. 10) presents no spectral features until frequencies between 600 and 800 cm^{-1} with a maximum at $\sim$670 cm^{-1}. Thus, the contribution of the distinct component produces a shift to higher frequencies of the librational band of the absorption

spectrum. A similar behavior of the distinct component was found in liquid water and it was ascribed to an optical-like mode.[42-44]

VII. SUMMARY

The static dielectric constant, the dielectric relaxation, as well as the infrared spectra of liquid ethanol at room conditions have been investigated from MD simulations. Two alternative ways to determine the dielectric properties have been considered. One of them consists in computing the total dipole moment fluctuations and time correlation functions. The other consists in obtaining the low k limit of the wave-vector dependent dielectric permittivity. The good agreement between the results obtained with the two approaches is an indication that our system can be considered as representing a real isotropic liquid. The behavior as a function of the wave-vector number of the transverse and longitudinal components of the static permittivity is in accordance with theoretical predictions. In particular, we have been able to find the singularity of $\epsilon_L(k)$ at small k. A different behavior for the time correlation functions of the longitudinal and transverse components of the dipole density has been observed. The $\Phi_L(k,t)$ functions decay faster than their transverse counterparts. For all the k values achieved in the simulations, both functions $\Phi_L(k,t)$ and $\Phi_T(k,t)$ show, at short times, an oscillatory behavior which is attributed to the librational dynamics of molecules. Computation of the self- and distinct contributions to the total dipole moment autocorrelation function have allowed us a better understanding of the physical origin of the different motions involved in the relaxation of the total dipole moment. The short-time behavior of $\Phi(t)$ is mainly due to single particle reorientations. On the contrary, the long-time decay of $\Phi(t)$ should be associated with collective motions. The dielectric relaxation bands computed from the simulations show a qualitative agreement with the experimental data, but the static dielectric constant and the dielectric relaxation times obtained from MD are smaller than the experimental ones. However, our results are in similar accordance with experiments reported for other hydrogen bonding liquids such as water and methanol. The infrared spectra shows a librational band with a peak at approximately $\simeq 640$ cm^{-1}. It is interesting to note that a nonnegligible contribution of the distinct component has been detected for frequencies between 600 and 800 cm^{-1}. In the far infrared region of the spectra, the self-component displays a maximum at frequencies $\simeq 70$ cm^{-1} which may be ascribed to the hindered motion of molecules in the cage of its neighbors.

ACKNOWLEDGMENTS

[1] B. M. Ladanyi and M. S. Skaf, Annu. Rev. Phys. Chem. **44**, 335 (1993).
[2] T. Fonseca and B. M. Ladanyi, J. Chem. Phys. **93**, 8148 (1990).
[3] J. Casulleras and E. Guàrdia, Mol. Simul. **8**, 273 (1992).
[4] M. S. Skaf, T. Fonseca, and B. M. Ladanyi, J. Chem. Phys. **98**, 8929 (1993).
[5] M. S. Skaf and B. M. Ladanyi, J. Chem. Phys. **102**, 6542 (1995).
[6] J. Barthel, K. Bachhuber, R. Buchner, and H. Hetzenauer, Chem. Phys. Lett. **165**, 369 (1990).
[7] J. T. Kindt and C. A. Schmuttenmaer, J. Phys. Chem. **100**, 10373 (1996).
[8] W. L. Jorgensen, J. Phys. Chem. **90**, 1276 (1986).
[9] M. E. van Leeuwen, Mol. Phys. **87**, 87 (1996).
[10] J. Gao, D. Habibollazadeh, and L. Shao, J. Phys. Chem. **99**, 16460 (1995).
[11] L. Saiz, J. A. Padró, and E. Guàrdia, J. Phys. Chem. B **101**, 78 (1997).
[12] J. A. Padró, L. Saiz, and E. Guàrdia, J. Mol. Struct. **416**, 243 (1997).
[13] M. A. González, E. Enciso, F. J. Bermejo, and M. Bée, J. Chem. Phys. **110**, 8045 (1999).
[14] P. Madden and D. Kivelson, Adv. Chem. Phys. **56**, 467 (1984).
[15] G. Stell, G. N. Patey, and J. S. Høye, Adv. Chem. Phys. **48**, 183 (1981).
[16] D. M. F. Edwards, P. A. Madden, and I. R. McDonald, Mol. Phys. **51**, 1141 (1984).
[17] M. Neumann, O. Steinhauser, and G. S. Pawley, Mol. Phys. **52**, 97 (1984).
[18] S. W. de Leeuw, J. W. Perram, and E. R. Smith, Annu. Rev. Phys. Chem. **37**, 245 (1986).
[19] *CRC Handbook of Chemistry and Physics*, 74th ed. (CRC, New York, 1994).
[20] H. J. C. Berendsen, J. P. M. Postma, W. F. van Gunsteren, A. DiNola, and J. R. Haak, J. Chem. Phys. **81**, 3684 (1984).
[21] J. P. Ryckaert, Mol. Phys. **55**, 549 (1985).
[22] M. P. Allen and D. J. Tildesley, *Computer Simulation of Liquids* (Oxford University Press, Oxford, 1987), Chap. 5.
[23] H. Flyvbjerg and H. G. Petersen, J. Chem. Phys. **91**, 461 (1989). See also, D. Frenkel and B. Smit, *Understanding Molecular Simulation. From Algorithms to Applications* (Academic, New York, 1996), Appendix D.
[24] A. Chandra and B. Bagchi, J. Chem. Phys. **90**, 1832 (1989); **91**, 3056 (1989).
[25] P. Attard, D. Wei, and G. N. Patey, Chem. Phys. Lett. **172**, 69 (1990).
[26] F. O. Raineri, H. Resat, and H. L. Friedman, J. Chem. Phys. **96**, 3068 (1992).
[27] P. A. Bopp, A. A. Kornyshev, and G. Sutmann, Phys. Rev. Lett. **76**, 1280 (1996).
[28] S. J. Rosenthal, R. Jiménez, G. R. Fleming, P. V. Kumer, and M. Maroncelli, J. Mol. Liq. **60**, 25 (1994), and references therein.
[29] D. Bertolini and A. Tani, Mol. Phys. **75**, 1065 (1992).
[30] D. Kivelson and H. L. Friedman, J. Phys. Chem. **93**, 7026 (1989).
[31] M. Neumann, J. Chem. Phys. **82**, 5663 (1985).
[32] The Debye limit corresponds to high friction and vanishing inertia.
[33] R. Buchner and J. Barthel, Annu. Rep. Prog. Chem. Sect. C: Phys. Chem. **91**, 71 (1994).
[34] L. Saiz, J. A. Padró, and E. Guàrdia, Mol. Phys. **97**, 897 (1999).
[35] D. A. McQuarrie, *Statistical Mechanics* (Harper & Row, New York, 1976), Chap. 21.
[36] C. F. L. Böttcher and P. Bordewijk, *Theory of Dielectric Polarization* (Elsevier, Amsterdam, 1978), Vol. 2.
[37] B. Guillot, P. Marteau, and J. Obriot, J. Chem. Phys. **93**, 6148 (1990).
[38] M. Falk and E. Whalley, J. Chem. Phys. **34**, 1554 (1961).
[39] J. Martí, J. A. Padró, and E. Guàrdia, J. Chem. Phys. **105**, 639 (1996).
[40] P. A. Madden and R. W. Impey, Chem. Phys. Lett. **123**, 502 (1986).
[41] G. E. Walrafen, in *Water, A Comprehensive Treatise*, edited by F. Franks (Plenum, New York, 1972), Chap. 5, Vol. 1.
[42] M. A. Ricci, D. Rocca, G. Ruocco, and R. Vallauri, Phys. Rev. A **40**, 7226 (1989).
[43] H. Resat, F. O. Raineri, and H. L. Friedman, J. Chem. Phys. **97**, 2618 (1992).
[44] D. Bertolini, A. Tani, and R. Vallauri, Mol. Phys. **73**, 69 (1991).